

# Doxazosin adsorption in natural, expanded, and organophilized vermiculite-rich clays

M. S. L. Rosa<sup>1\*</sup>, R. A. O. Silva<sup>1</sup>, P. A. A. e Sousa<sup>1</sup>, R. T. do Nascimento<sup>1</sup>, T. Knoerzer<sup>2</sup>, M. R. M. C. Santos<sup>1</sup>

<sup>1</sup>Federal University of Piauí, Center of Natural Sciences, 64049-550, Terezina, PI, Brazil

<sup>2</sup>US Air Force Academy, Department of Chemistry, CO 80840, USA

## Abstract

Vermiculite clays are adsorbent materials that have good chemical adsorption capacity, which makes them applicable in the removal of drugs from aqueous solutions. Their lamellar structure can be easily expanded and organophilized. To assess the efficacy and environmentally-tolerant capacity of the adsorption method, the organophilized vermiculite clay was compared to both natural and expanded vermiculite clays. To prepare the organophilized clays, a natural clay sample was expanded at 900 °C. The expanded clay was thus treated by immersion in a 1.0 M NaCl solution and organophilized using a cetyltrimethylammonium bromide (CTMA-Br) surfactant, for 24 h at 50 °C. Natural, expanded, and organophilized samples were characterized using the techniques of XRD, FTIR, TG/DSC, and SEM to observe structural changes after expansion and organophilization. These characterizations indicated that there was an increase in the interlamellar space of the expanded and organophilized sample. In addition, a study of the point of zero charge was performed to determine the surface changes of the samples and the amount of doxazosin adsorption in the samples was determined by the time adsorption test. Further, the organophilized sample showed potential adsorption of the drug doxazosin and high performance in relation to the expanded and natural samples.

**Keywords:** clay, adsorption, drug, doxazosin.

## INTRODUCTION

The expansive development of pharmaceutical industries through the 20<sup>th</sup> and 21<sup>st</sup> centuries has resulted in the disposal of drugs in urban sewage systems leading to observed environmental problems [1]. Of primary importance is the fact that pharmaceutical wastes persist for a long time and are not completely removed in sewage treatment plants (STPs), leading to the prevalence of toxic, carcinogenic, and persistent drugs in water supplies [2]. In addition to these problems related to drug prevalence in the aquatic environment, a recent report suggests that a primary water-polluting source is hospital effluents with discharges of various drugs potentially leading to the unintentional development of bacterial resistance, which may ultimately lead to an estimated 10 million deaths per year by 2050 worldwide [3]. Consequently, a distinct need exists for the remediation of effluents to promote the effective removal of drug-related waste. The primary means of remediation include coagulation and flocculation, advanced oxidative processes, use of membranes by nanofiltration, microbial treatment, and adsorption [4-6]. In fact, adsorption is the cheapest and most environmentally viable method as it uses adsorbent materials such as clays and lignocellulosic compounds that are readily found in nature [7, 8]. Moreover, these materials have been shown to adsorb organic and inorganic compounds, such as drugs, dyes, and heavy metal ions (Cr, Pb, Ni, among others). Among these materials, clays have become particularly attractive because of their

low cost, lack of toxicity, and wide natural availability. In addition, clays may contain other weathered minerals, such as hydrobiotite, mica, and vermiculite that contain a fraction of the negative charge in the structure responsible for adsorption of the contaminant [8]. In addition, clays have a large surface area, which contributes to their high adsorption capacity and, consequently, adsorption of drugs such as antihistamines, antipsychotics, cytostatics, gastrointestinal, lipid regulators, sedatives, and  $\alpha$ -adrenergic selective blockers, such as doxazosin [9, 10]. Doxazosin mesylate is a uniquely interesting remediation target due to its use for the treatment of benign prostatic hyperplasia [11]. The standard dosing regimen varies from 1 to 16 mg/day and the pharmacokinetic profile is linearized within the therapeutic dosage range [11]. As a result, substantial plasma levels of the drug can be expected upon dosing, therefore, leading to potential drug accumulation and eventual presence of the drug in human excretion. By extension, doxazosin has a high probability of detection in hospital effluents and is likely an ideal candidate for evaluating its remediation by adsorption into clays.

In order to improve the drug adsorption process, previous studies have shown that effective methods include clay expansion at temperatures above 300 °C (Fig. 1a) and organophilization of clays with the use of sodium chloride solution (aq) with surfactants (Fig. 1b) [12, 13]. In expanded and organophilized clays, there is often concomitant exfoliation and therefore, an increase in the number of pores on the surfaces of the lamellae may ensure greater adsorption of an organic compound. In addition, during clay organofunctionalization, the substitution of exchangeable monovalent cations present in the space that exists between

\*mirnasales01@hotmail.com

 <https://orcid.org/0000-0003-3509-9824>

the layers by organic cations of quaternary ammonium salts assists the insertion of long organic chains between the clay mineral layers rendering a material transformation from hydrophilic to organophilic, which ultimately favors the process of adsorption of organic compounds [8-14]. The adsorption process of organic compounds such as the drug doxazosin is illustrated in Fig. 1c. The adsorption process is often reversible so that with the change in temperature and/or pressure, hydrogen potential can cause easy removal of the adsorbed solute in the solid [15, 16]. Thus, the study of parameters such as time, pH, and temperature must be used in adsorption tests to guarantee the effectiveness of the process [17, 18]. Herein, we present the preparation and analysis of a newly developed organophilic clay that holds the excellent potential to be used as an effective remediation agent especially as it applies to the removal of pharmaceutical agents in wastewater and adsorption tests using the physical-chemical parameters of time and pH.

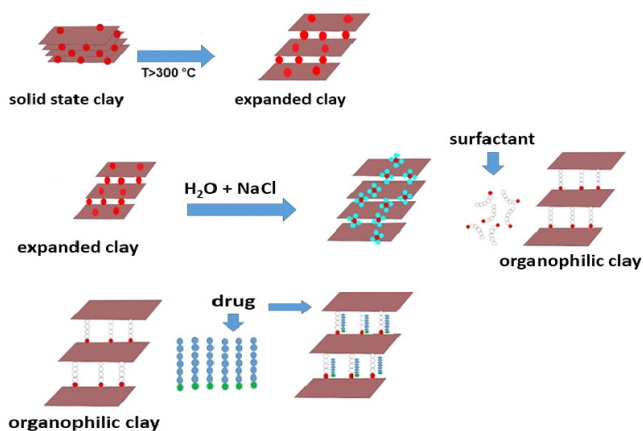


Figure 1: Illustration of: a) vermiculite clay expansion at temperatures above 300 °C; b) organophilization of vermiculite clays with the use of sodium chloride solution (aq) with surfactants; and c) adsorption process of the drug.

## MATERIALS AND METHODS

**Vermiculite clay preparation:** natural vermiculite clay (NC) was collected near a lake in the city of Caxias, State of Maranhão, Brazil. Initially, the natural clay was submitted to the manual quartering process to obtain a more homogeneous final sample. The NC was ground and macerated with a mortar and porcelain pestle. Subsequently, the sample was sieved through a 125 mesh sieve to provide the necessary fine material for the next phase of preparation. **Elimination of clay's organic matter:** initially, NC (10 g) was treated with enough distilled water to moisten the sample and then  $H_2O_2$  (30 mL) was added to the moistened clay. The sample was heated to 80 °C for 20 min until hydrogen peroxide evaporation ceased. The remaining solid was then washed with distilled water (3x) and centrifuged at 800 rpm for 10 min following each water treatment. Finally, the material was dried on a stove at 100 °C for 2 h. **Vermiculite**

**clay expansion:** the previously prepared NC (20 g) was placed in crucibles and then heated in a muffle oven for 15 min at around 900 °C to provide the expanded clay (EC). **Obtaining monosodium clay:** EC (1 g per 400 mL of aqueous 1 M NaCl solution) was introduced to a 1 L round-bottom flask affixed with a water-cooled condenser. The mixture was heated by an oil bath set at 50 °C for 72 h. Upon completion, the material was centrifuged several times from distilled water for 30 min with a rotation speed of 3500 rpm until total removal of chloride anions. The remaining solid material was kiln-dried at 60 °C for 24 h. The dry material was ground and sieved with a 125 mesh sieve to provide the monosodium clay (MSC). **Obtaining the organophilic clay:** a 250 mL round bottom flask was charged with MSC (15 g), 100 mL of distilled water, and cetyltrimethylammonium bromide (CTMA-Br, 6 g). The resulting mixture was heated for 24 h at 50 °C. Subsequently, the mixture was filtered, washed with distilled water, and dried in an oven at 60 °C for 48 h. The dried material was ground and sieved with a 125 mesh sieve to provide the organophilic clay (OC). **Conversion of doxazosin mesylate to doxazosin free amine:** doxazosin was prepared from doxazosin mesylate based on a previously published methodology [19]. Doxazosin mesylate (5 g) was dissolved in 250 mL of deionized water with stirring for 30 min. The pH of the system was adjusted to 12 by the careful addition of 1.0 M NaOH, which resulted in the precipitation of DOXA free amine. The solid material (DOXA) was isolated by vacuum filtration and the filter cake was washed with an additional 520 mL of deionized water. The remaining solid material was air-dried for 72 h and macerated.

**X-ray fluorescence spectroscopy (XRF):** the XRF elemental analysis was performed to determine the main constituents present in clay samples. The content of the primary oxides was determined by a semi-quantitative analysis using a Thermo Fisher Scientific, Niton XL3t Ultra X-ray fluorescence spectrometer equipped with an X-ray tube, a silver anode, and a silicon drift detector (SDD). The instrument was equipped with an X-ray tube of 50 kV maximum voltage, 200  $\mu$ A current, and 2 W of power. The samples were placed in a 32 mm collimator with 2.5" diameter and 4  $\mu$ m thick polypropylene film using a focal point of 3 mm in diameter. Analysis time was set to 120 s and all acquisitions were performed under a nitrogen atmosphere. Results were expressed as oxide contents. **X-ray diffraction (XRD):** crystallographic profiles of natural, expanded, and organophilized clay were obtained using a Shimadzu XRD-6000 X-ray diffractometer, using  $CuK\alpha$  radiation ( $\lambda=1.5406 \text{ \AA}$ ). Each analysis was performed operating in the  $2\theta$  range of 3-80° and scanning rate of 2  $^\circ$ .min<sup>-1</sup> for a 40 min exposure period. XRD patterns were compared with the crystallographic data of the HighScore JCPD program to determine the crystalline phases. **Fourier transform infrared spectroscopy (FTIR):** clarification of structural changes of the adsorbent was determined by infrared spectroscopy using a Bruker Vertex 70 instrument. Samples were prepared as KBr pellets and acquisition

conditions included a spectral range from 4000 to 400  $\text{cm}^{-1}$ , with 64 total scans at 4  $\text{cm}^{-1}$  resolution. *Thermal analysis*: the analysis of the samples was performed by thermogravimetry (TG) and differential scanning calorimetry (DSC) using a TA Instruments, Q600 SDT system. Samples (~9.75 mg) were evaluated under a nitrogen atmosphere in the 10 to 1000 °C range with a heating rate of 10 °C.min<sup>-1</sup>. *Scanning electron microscopy (SEM)*: particle morphology of the samples before and after expansion and organophilization was evaluated using an FEI Quanta FEG 250 scanning electron microscope. Micrographs were obtained by operating the microscope using metallic support (stub) with a double-sided carbon tape for powder fixation and after metallization of the samples with gold. *Kinetic study*: to investigate the influence of time on adsorption, tests were performed with 40.0 mL of the 70.0  $\text{mg}\cdot\text{L}^{-1}$  DOXA solutions and 20.0 mg of NC, EC, and OC. The system was kept under agitation at 25 °C for different contact times (30 to 1440 min) at the best pH. Thereafter, drug concentration in the supernatant was determined by UV-visible spectroscopy using a Cary 60 UV-Vis spectrometer. All experiments were performed in triplicate, and the adsorption capacity of samples NC, EC, and OC was calculated by:

$$q = \frac{C_1 - C_2}{m} v \quad (\text{A})$$

where  $q$  is the amount of adsorption of doxazosin ( $\text{mg}/\text{g}$ ),  $C_1$  is the initial concentration of doxazosin before adsorption ( $\text{mg}/\text{L}$ ),  $C_2$  is the final concentration of doxazosin after adsorption in adsorbent materials ( $\text{mg}/\text{L}$ ),  $m$  is the adsorbent mass ( $\text{mg}$ ), and  $v$  is the volume of the drug solution [19, 20]. The experimental data of the time influence isotherm were fitted to two kinetic models, pseudo-first-order and pseudo-second-order at equilibrium time. For the pseudo-first-order model [21, 22], Eq. B was applied:

$$\log(q_{e,\text{exp}} - q_t) = \log(q_{e,\text{theo}}) - \frac{K_1}{2.303} t \quad (\text{B})$$

where  $q_{e,\text{exp}}$  ( $\text{mg}/\text{g}$ ) is the amount adsorbed per gram of adsorbent in balance,  $q_{e,\text{theo}}$  is the theoretical adsorbed amount per gram of adsorbents,  $q_t$  is the amount adsorbed per gram of adsorbent in time  $t$  (min), and  $K_1$  ( $1/\text{min}$ ) is the pseudo-first-order adsorption speed constant. To obtain the parameters of the pseudo-first-order equation, a graph ( $q_{e,\text{exp}}$  versus  $K_1$ ) was plotted and from this plot, the angular and linear coefficients were extracted. For the pseudo-second-order model [8-22], the following equation was used:

$$\frac{t}{q_t} = \frac{t}{K_2 \cdot q_{e,\text{theo}}^2} + \frac{t}{q_{e,\text{theo}}} \log(q_{e,\text{theo}}) - \frac{k_1}{2.303} t \quad h = K_2 \cdot q_{e,\text{theo}}^2 \quad (\text{C})$$

where  $K_2$  is the pseudo-second-order velocity constant ( $1/\text{min}$ ) and  $h$  is  $q_t/t$ . All other variables are as defined for the pseudo-first-order equation above. *pH influence*: the influence of pH on the adsorption was studied for different pH values (1 to 10). Then, 20.0 mg of the adsorbent were placed in 40.0 mL

of a 70.0  $\text{mg}\cdot\text{L}^{-1}$  DOXA aqueous solution and stirred for 120 min at 25 °C. Subsequently, the material was centrifuged, and the final DOXA concentration in the supernatant was determined by the equation of the adsorption capacity of samples NC, EC, and OC. *Point of zero charge ( $\text{pH}_{\text{pzc}}$ )*: the  $\text{pH}_{\text{pzc}}$  of the NC, EC, and OC clays was determined by the method of adding solids. In a typical procedure, 25.0 mL of a 0.1 M solution of potassium nitrate ( $\text{KNO}_3$ ) was added to 36 Falcon tubes. The initial pH ( $\text{pH}_i$ ) was adjusted between 1 to 10 by the selected addition of 0.1 M HCl for acidification and 0.1 M NaOH for basification. After pH adjustment, 20.0 mL aliquots were taken from each flask and transferred to an Erlenmeyer flask containing 20.0 mg of adsorbents (NC, EC, and OC). The system was placed under agitation for 24 h at 25 °C. Subsequently, the material was centrifuged and pH measurements were performed in the supernatant obtaining the final pH of the solution ( $\text{pH}_f$ ). The difference between  $\text{pH}_i$  and  $\text{pH}_f$  was calculated ( $\Delta\text{pH} = \text{pH}_i - \text{pH}_f$ ) and a plot of  $\Delta\text{pH}$  as a function of  $\text{pH}_i$  was constructed to determine the  $\text{pH}_{\text{pzc}}$  [11, 12].

## RESULTS AND DISCUSSION

*X-ray fluorescence spectroscopy (XRF)*: XRF was conducted as an initial probe of vermiculite clay composition in order to identify the specific type of clay that was manipulated in our experimental process. According to the results of chemical compositions (Table I), vermiculite was primarily comprised of silica ( $\text{SiO}_2$ ), alumina ( $\text{Al}_2\text{O}_3$ ), and magnesia ( $\text{MgO}$ ). Leveraging the results compiled in a previous study [23], our results, based upon the Mg and Al content, suggested the presence of the crystalline phase of vermiculite, which has structural similarities with both chlorite  $(\text{Si,Al})_8(\text{Mg,Fe})_6\text{O}_{20}(\text{OH})_4$  and montmorillonite  $\text{Al}_4\text{Si}_8\text{O}_{20}(\text{OH})_4 \cdot n\text{H}_2\text{O}$  ( $n$  = interlamellar water) [24-27]. Moreover, the smaller percentages of the constituents CaO and  $\text{K}_2\text{O}$  suggested that the potassium ion was probably intercalated with mica, but this potassium was not exchangeable. Some of the magnesium ions were probably also exchangeable ions in vermiculite. Taken altogether, the total oxides of chemical analysis percentage values for clay composition summate to a value of 86.18%; the remaining amount of 13.38% was determined by loss on ignition, which can be attributed to the adsorbed water, possibly to organic matter, and condensation of structural hydroxyl groups of the octahedral sheet structure of clay minerals [23-27].

*XRD analysis*: the X-ray diffraction patterns of the samples (Fig. 2) demonstrated reflections that are typically indexed for vermiculite, mica, hydrobiotite, and quartz. The characteristic peaks of vermiculite appeared at 7.23°, 36.29°, 46.21°, 64.35°, and 71.18° of  $2\theta$  according to the reference file JCPDS 29-1499. The main peak at 7.23°  $2\theta$  was consistent with the interstratified phase (biotite-vermiculite), called hydrobiotite. The presence of mica was also apparent at 8.04°  $2\theta$  (9.9 Å) according to the reference file JCPDS 74608 [28-31]. It was possible to observe peaks at 3.02°, 41.02°, and 43.96°  $2\theta$ , corresponding to basal distances of

Table I - Chemical composition (wt%) of vermiculite clay as determined by X-ray fluorescence spectroscopy.

SiO <sub>2</sub>	MgO	Fe <sub>2</sub> O <sub>3</sub>	Al <sub>2</sub> O <sub>3</sub>	CaO	K <sub>2</sub> O	TiO <sub>2</sub>	LOI	Total
39.75	15.82	10.98	11.54	3.18	3.49	1.42	13.38	99.56

LOI: loss on ignition.

29.23, 1.17, and 2.78 Å, respectively, which may be further illustrative of the mineral hydrobiotite, which is formed in the conversion process to vermiculite and is ascribed to the hydration of phlogopite/biotite by weathering water on the surface of weathered rocks [29]. The presence of quartz was identified by peaks at 22.70° (3.4 Å) and 28.84° (3.0 Å), whose main peak is at 3.4 Å according to the reference file ICSD 01-079-1910, which confirmed other works [27, 28, 31-33].

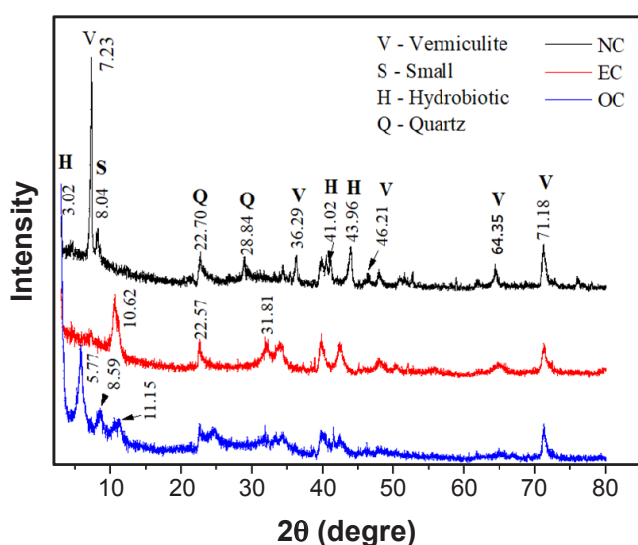


Figure 2: XRD patterns of natural (NC), expanded (EC), and organophilic (OC) vermiculite clays.

The diffractogram (Fig. 2) of EC showed the same characteristic peaks observed in NC, but it was observed the disappearance of the main peak at  $2\theta=7.23^\circ$  that must have been the result of the rapid loss of interlamellar water, which disturbs the stacking of the layers along with the crystallographic axis *c*. It is noteworthy to observe the displacement of the peak from  $2\theta=7.23^\circ$  present in the NC to  $2\theta=10.62^\circ$  (EC), which suggested that during the expansion process there was disorganization of the vermiculite layers [33-35]. On the analysis of X-ray diffraction of OC, it was possible to identify the displacement of the peak at  $7.23^\circ$   $2\theta$  of NC compared to the peak of OC at  $5.77^\circ$   $2\theta$ . This displacement to smaller angles indicated that there was an increase in the lamellar space from 12.24 Å in NC to 15.32 Å in OC. Furthermore, the OC structure was supported by the appearance of a distinct peak for OC at  $11.15^\circ$ , which correlated with a basal distance of 7.96 Å, and according to Alvarenga et al. [18] probably represents differences in the orientation of ammonium salt between the clay layers as well as an increase in the distance between the silicate layers.

According to Katiane et al. [12], the appearance of new peaks in OC may also be associated with adsorbed water, which causes a separation of layers. For the adsorptive study of this work, it is important to highlight that the presence of quartz and mica in clay possibly reduced the adsorption capacity of cationic groups because these minerals lack cation exchange capacity in relation to samples modified by the expansion and organophilization process [34].

**Thermal analysis:** thermogravimetric analysis (TG) and differential scanning calorimetry (DSC, Fig.3) provided information on the changes that occurred in the NC, EC, and OC samples as a result of heat and chemical treatment, as well as the mass loss interval and the physicochemical processes that involved energy variation. In natural clay (NC, Fig. 3a), the first TG event occurred in the 20-102 °C range with a mass loss of 8.60%, characterized by the evaporation of water adsorbed on the vermiculite clay surface [34]. The second event with a mass loss of 1.08% occurred in the 102-200 °C range, which can be attributed to the detachment of coordinating water by hydrogen bonding present in the interlamellar space of the vermiculite structure. The last event in the 200-530 °C range with a mass loss of 2.07% was likely due to dehydroxylation of the material, which is ascribed to the condensation of the silanol groups resulting from the release of water molecules [35]. The DSC curve confirmed the three events mentioned above as apparent endothermic peaks in the same temperature range of mass loss observed in the TG curve. The three peaks were likewise attributed to the losses of adsorbed water, followed by coordination of water, and finally dehydroxylation of the material [32].

In expanded clay (EC, Fig. 3b), a similar series of three endothermic events was observed in the TG profile. Congruent with the results of NC, there was a mass loss of 1.96% between 19 and 98 °C characteristic of the evaporation of adsorbed water on the surface of the material. The second thermal event occurred at around 98-190 °C with a mass loss of 2.55% corresponding to the water outflow of the interlamellar space of the vermiculite clay. The third event took place at 190-450 °C, which again can be explained as dehydroxylation of the material. It can be inferred that the shift toward lower temperature in the TG profile was probably due to the predisposed loss of water with a temperature that would have occurred upon clay expansion and is consistent with previously observed results [32]. Parallel to the results for NC, the EC sample showed the expected endothermic transitions within the corresponding DSC data albeit with modification of the exothermic tailing seen in the NC sample for temperatures beyond 600 °C. Perhaps the phase change occurred at higher temperatures (>800 °C, Fig. 2b).

In organophilized clay (OC, Fig. 2c) the TG/DSC

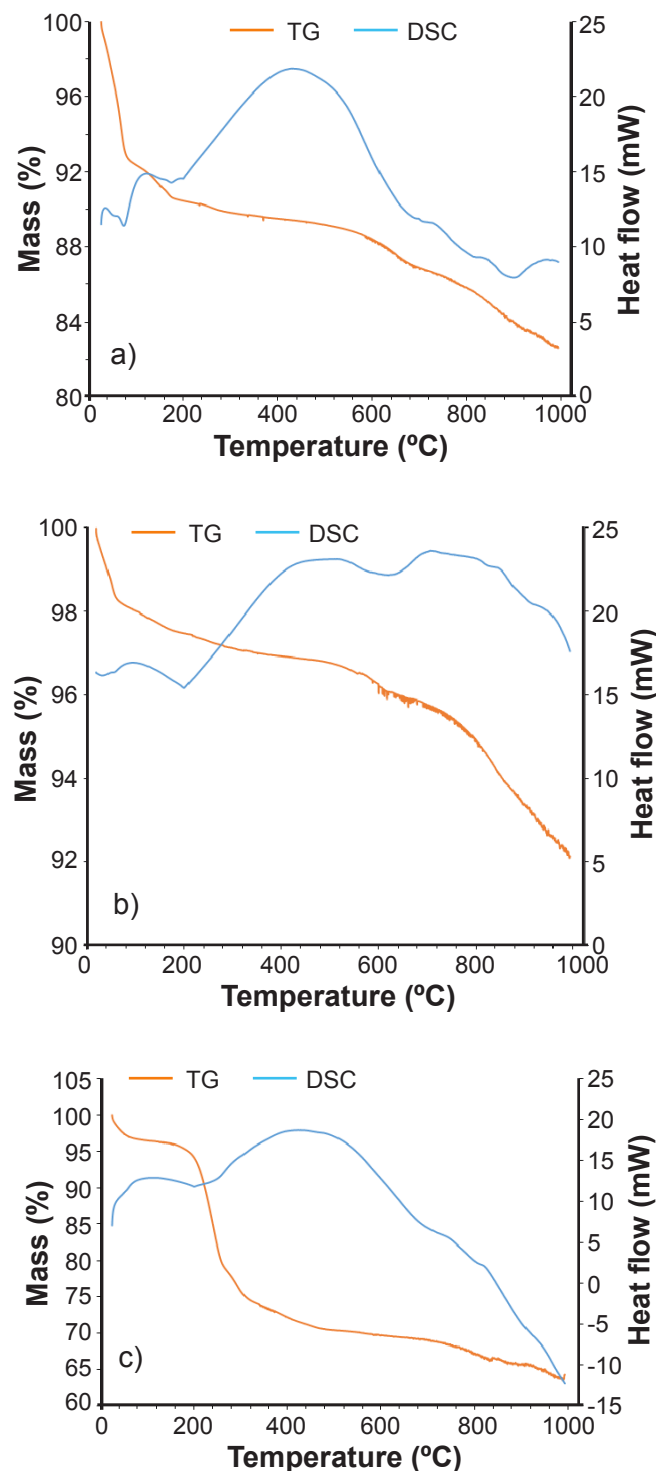


Figure 3: Thermogravimetric (TG) and differential scanning calorimetry (DSC) curves for NC (a), EC (b), and OC (c).

curves also showed mass loss ranges initially at around 25-96 °C with a mass loss equal to 3.44% corresponding to surface water dehydration. This event was congruent with the results for both NC and EC samples. Similarly, the range of 96-205 °C produced a mass loss of 2.47%, which was related to the dehydration of interlamellar water molecules. Alternatively and to our delight, the range of

205-434 °C demonstrated a considerable difference in mass loss (10.51%), which was expected and was characteristic of the decomposition of ammonium salt providing strong evidence for the formation of the OC. At temperatures beyond 434 °C, a final decomposition of organic salt was observed. Overall, OC showed lower thermal stability than NC and EC samples as evidenced by the severe precipitous drop in the TG profile in the 205-434 °C range. The studies corroborated the results presented by Ho and McKay [25], who observed this decrease in thermal stability due to the presence of surfactant alkylammonium ions that degrade at lower temperatures and affect the stability of the material. The number of events and their respective mass losses found and total mass losses (TML) in the thermal analysis of the samples, NC, EC, and OC are summarized in Table II.

**FTIR analysis:** the infrared spectrum (Fig. 4) was performed to obtain qualitative identification of functional groups. For NC, a wide and intense absorption band was observed in the region of 3428  $\text{cm}^{-1}$  (Fig. 4a) corresponding to axial vibrations of silanol groups (Si-OH) of the structure and also characteristic of water molecules that are adsorbed by hydrogen bonds found in the interlamellar region [27]. Moreover, in this same region, there was a small congruent displacement in the region of 3438  $\text{cm}^{-1}$  for the samples EC (Fig. 4b) and OC (Fig. 4c). A mean absorption band in the spectrum in the region of 1638  $\text{cm}^{-1}$  was seen in all three samples, which was attributed to the symmetrical angular deformation of the O-H water bond, confirming the presence of water in the structure of the natural and modified materials. Another strong intensity band at 1006  $\text{cm}^{-1}$  was observed in the spectrum of NC (Fig. 4a) and at 1010  $\text{cm}^{-1}$  for the EC (Fig. 4b) and OC (Fig. 4c) samples corresponding to the asymmetric stretching region of Si-O-Si and Si-O-Al of the tetrahedral and octahedral layers [32, 43]. According to Franco et al. [35], weak intensity bands were observed at 679  $\text{cm}^{-1}$  in all samples, which can be assigned to Si-O deformation vibrations, likely to be related to Si-O-M bending vibrations (M=Fe,Al,Mg) that would be expected in the materials presented here. All three samples also revealed an average intensity band at 448  $\text{cm}^{-1}$ , which was attributed to the deformation vibration of the Si-O-Si siloxane groups of the groups  $[\text{Si}_2\text{O}_5]$ . FTIR analysis further afforded the identification of the modified vermiculite clay material and key evidence for the efficiency of the organophilization reaction. In particular, for the OC sample (Fig. 4c), a difference was the appearance of new characteristic bands of ammonium salt at 2918 and 2849  $\text{cm}^{-1}$ , which were assigned to symmetric and asymmetric stretches of  $\text{CH}_2$  groups, respectively. In addition, the appearance of the peak at 1471  $\text{cm}^{-1}$  further supported organofunctionalization and was due to the bending vibrations of groups  $\text{CH}_3$ . This observation was corroborated by Dlugosz and Banach [44] and was consistent with the presence of surfactant hydrophobic chain peaks. Further corroboration is provided by other studies [46-48], which reported that these absorptions are characteristic of clay minerals organofunctionalized with alkoxysilanes of different functionalities such as amino,

Table II - Results of thermal analysis of adsorbing materials.

Sample	1 <sup>st</sup> event	ML <sub>1</sub> (%)	2 <sup>nd</sup> event	ML <sub>2</sub> (%)	3 <sup>rd</sup> event	ML <sub>3</sub> (%)	TML (%)
NC	20-102 °C	8.60	102-200 °C	1.08	200-530 °C	2.07	11.75
EC	19-98 °C	1.96	98-190 °C	2.55	190-450 °C	2.69	7.20
OC	25-96 °C	3.44	96-205 °C	2.47	205-434 °C	10.51	16.42

ML: mass loss; TML: total mass loss.

mercapto, and epoxy groups. FTIR also showed the decrease in band intensity at 1638 cm<sup>-1</sup> for OC versus NC or EC (Fig. 4), which presumably corresponded to the presence of water coordinated with the exchangeable cations of clay. This result is important as it showed evidence for the effective incorporation of surfactant within the structure of the material. Finally, the FTIR data were congruent with the results obtained by the XRD and supported the efficacy of the surfactant intercalation process in the vermiculite clay structure.

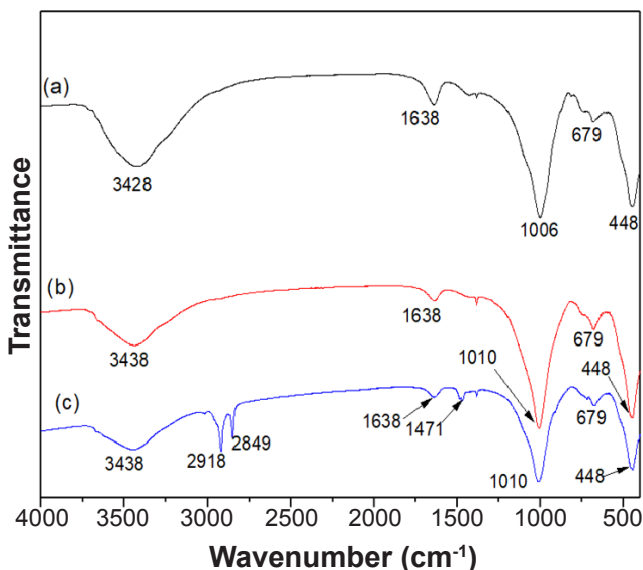


Figure 4: FTIR spectra of the samples: a) NC; b) EC; and c) OC

**Scanning electron microscopy:** SEM analysis provided more information on the morphology of vermiculite clay before and after the heat and chemical treatment. Fig. 5 shows the electron microscopy images of the NC, EC, and OC samples. In Figs. 5a and 5b for NC, there is a compact lamellar structure arranged in overlapping layer blocks. According to Da Silva et al. [37], there is also a structure composed of larger lamellae covered with smaller particles in the microstructure of natural vermiculite clay. In Fig. 5c, for EC, the lamellar structure of expanded vermiculite clay is observed with morphology showing the presence of plaques and exfoliations due to the vaporization of water from the layers during the expansion process (as noted in similar, expanded materials studied by Rojas-Ramires et al. [29]). For OC (Figs. 5d and 5e), we observed more consistent and scaly clusters that probably arose from the grouping of particles and filling of layers by organic salt

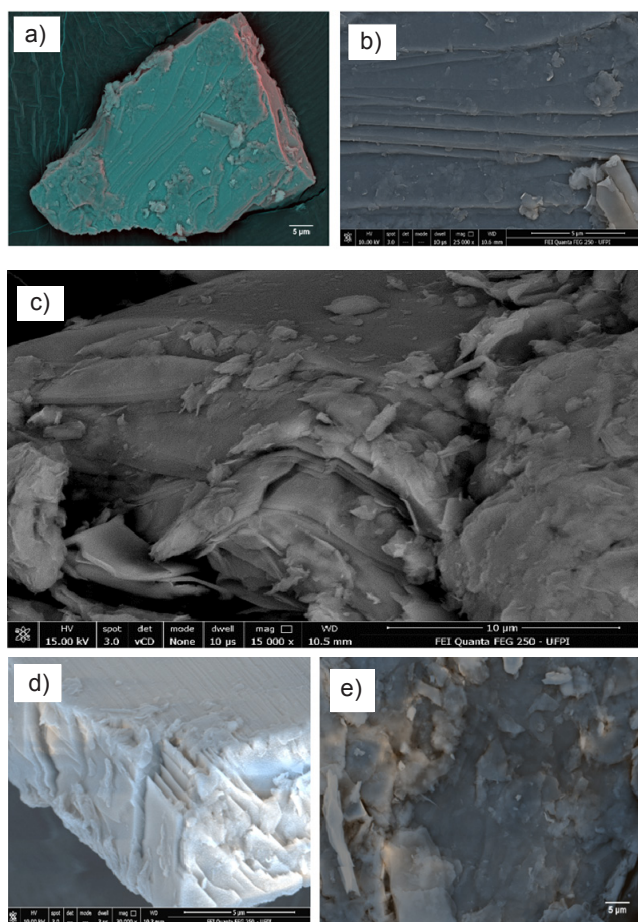


Figure 5: SEM micrographs of the samples NC (a,b), EC (c), and OC (d,e).

surfactant molecules. This observation for the OC sample was consistent with the work of Tang et al. [43], who demonstrated that the organophilization of vermiculite clay with CTMA-Br salt afforded improvements indicating the possibility of an increase in the sorption capacity of organic pollutants due to the increase in the interlamellar space of the clay. Likewise, another investigation [44] also has described the introduction of organic surfactants in the lamellar structure of clay, which resulted in material activation favoring the increase of the adsorption process.

**Effect of pH on adsorption of doxazosin:** the maximum adsorption capacity of the NC, EC, and OC for DOXA at different pH values was studied, and the results are compared in Fig. 6. Above the pH<sub>pzc</sub>, the vermiculite clay surface would be expected to possess excess negative charge loading (nominally OH<sup>-</sup> groups), which favors adsorption of

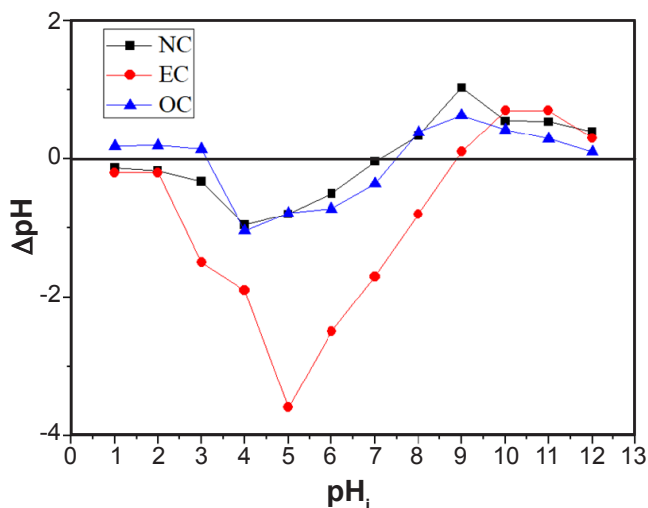


Figure 6: Plot of the difference between initial and final pH ( $\Delta\text{pH}$ ) in the doxazosin adsorption tests as a function of initial pH ( $\text{pH}_i$ ) for determination of the  $\text{pH}_{\text{pzc}}$  of NC, EC, and OC samples.

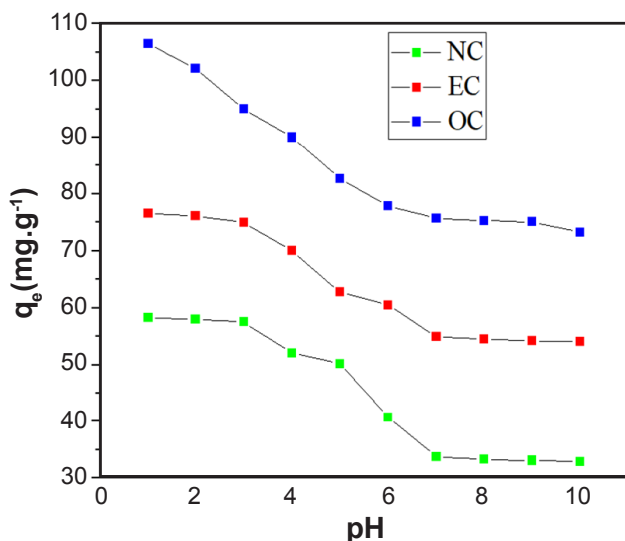


Figure 7: pH-dependent isotherm for removing doxazosin in the NC, EC, and OC samples.

cationic groups. Below the  $\text{pH}_{\text{pzc}}$ , the vermiculite surface has a predominantly positive charge (nominally  $\text{H}^+$  groups) favoring the adsorption of anionic groups [11-46]. The pH is

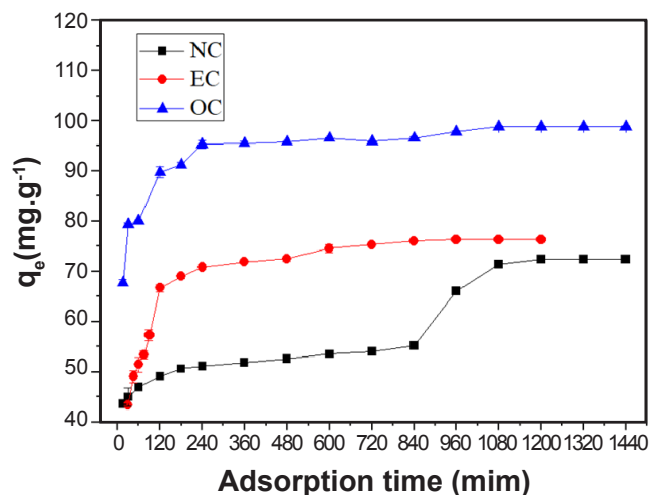


Figure 8: Time-dependent isotherm for doxazosin removal in NC, EC, and OC samples.

an important parameter in the adsorption process of organic materials because the solubility of the adsorbate in solution and the load of the active sites on the surface of the material can change depending on the pH value. Data from the study of the pH of the NC, EC, and OC samples are shown in Fig. 7, with a  $q_e$  (amount of adsorption of doxazosin) curve as a function of pH. The adsorption of doxazosin on the surface of NC, EC, and OC was clearly influenced by pH as demonstrated by the downward deflection with increasing pH values. It can be seen that the maximum adsorption in the NC clay was at pH equal to 1 ( $58.29 \text{ mg.g}^{-1}$ ), but little variance was observed up to a pH value of 3. In relation to the adsorption in EC, as the pH increased, there was also a steady region for adsorption of the drug in the vermiculite clay up to a pH equal to 3 ( $76.02 \text{ mg.g}^{-1}$ ). For OC, the maximum adsorption occurred at pH equal to 1 ( $106.42 \text{ mg.g}^{-1}$ ) and showed an immediate decrease in adsorption for pH values higher than 1. These findings can be explained based upon how the alteration in pH can act to change the surface charge of the vermiculite clay, by way of the protonation or deprotonation of the silanol groups ( $\text{Si-OH}$ ). At acidic pH, the increase in the amount of DOXA adsorbed on the NC, EC, and OC was related to the decrease in electrostatic repulsion between the hydroxyl groups on the

Table III - Kinetic parameters obtained with the pseudo-first-order and pseudo-second-order equations for adsorption of the drug DXZ in NC, EC, and OC vermiculite clays.

Adsorbent	Kinetic model	$q_{e,\text{exp.}}$ ( $\text{mg.g}^{-1}$ )	$q_{e,\text{calc.}}$ ( $\text{mg.g}^{-1}$ )	$k_1$ ( $\text{g.mg}^{-1}.\text{min}^{-1}$ )	$k_2$ ( $\text{g.mg}^{-1}.\text{min}^{-1}$ )	$R^2$
Natural clay	Pseudo-first-order	72.405	35.320	0.00186	-	0.5423
	Pseudo-second-order	72.405	73.583	-	0.1335	0.9999
Expanded clay	Pseudo-first-order	76.333	27.431	0.00510	-	0.9389
	Pseudo-second-order	76.333	78.308	-	0.0004	0.9999
Organophilized clay	Pseudo-first-order	98.828	24.872	0.00450	-	0.8897
	Pseudo-second-order	98.828	99.502	-	0.7105	0.9998

protonated clay surface and the protonated nitrogen groups of DOXA [11-40].

**Kinetic study:** with the characterization features defined, the application of the material with respect to doxazosin adsorption was explored. Fig. 8 shows the variation of doxazosin adsorption as a function of the time of contact with NC, EC, and OC. As a matter of design, careful attention was paid to the time needed to achieve the adsorption balance in order to properly ascertain the affinity of the adsorbent with an adsorbate. To determine adsorption isotherms, it is necessary that the contact time between the adsorbent and the adsorption is sufficient to achieve this adsorption equilibrium. The process equilibrium occurs when the adsorbent reaches saturation, that is, the moment that there is no more adsorption of the compound, where the adsorption rate is the same as that of desorption [22, 23]. As shown in Fig. 8, the adsorption speed of doxazosin (DXZ) in NC, EC, and OC was faster in the early stages of the process (up to 240 min), and then slowed to the equilibrium phase (later than 240 min). This behavior occurred because, in the beginning, there was a large number of sites available for adsorption [44, 45]. Over time, the adsorption of doxazosin (expressed as  $q_e$  or mg of DXZ per g material) slowed due to the gradual occupation of the available sites, decreasing the observed speed of the adsorption process. This process continued until reaching equilibrium. From the results, the equilibrium time in the NC occurred after 1080 min, reaching an adsorption balance in the time of 1440 min at an adsorption rate of 72.40 mg.g<sup>-1</sup>. For the EC, the adsorption equilibrium time occurred after 720 min, with an adsorption balance of 1200 min (76 mg.g<sup>-1</sup> of adsorption) and for the OC, the equilibrium time occurred after 960 min, reaching a balance in the time of 1440 min (98.81 mg.g<sup>-1</sup> of adsorption). Comparable degrees of adsorption balance were achieved with NC and EC, but the efficacy was increased considerably for OC (98.81 mg.g<sup>-1</sup>), thus demonstrating the functional capacity of the organophilized material.

Further evidence was provided by kinetic analysis of adsorption. The experimental kinetic data (Table III) of adsorbing the drug DXZ in relation to the vermiculite clays were submitted to a mathematical treatment by means of the pseudo-first-order and pseudo-second-order kinetic models. For each kinetic study of the adsorption of the drug DXZ in NC, EC, and OC, the pseudo-second-order model showed the best fit for the adsorption process due to the highest values of the correlation coefficient with a value of  $R^2=0.9999$  for NC,  $R^2=0.9999$  for EC, and  $R^2=0.9998$  for OC in relation to the pseudo-first-order model. Presumably, the rate-limiting step in this process was the chemisorption of the drug on the surface of the OC material, thus showing consistency with the pseudo-second-order model [47]. In this process, there is the donation or exchange of electrons between adsorbate and adsorbent by way of covalent and ion exchange forces [25].

## CONCLUSIONS

We have demonstrated the efficient synthesis of organophilic clay (OC) from monosodium vermiculite clay

(MSC) and cetyltrimethylammonium bromide (CTMA-Br) for the effective adsorption of the doxazosin (DXZ) drug. Natural clay (NC), expanded clay (EC), and OC characteristics were evaluated and confirmed by XRF, XRD, TG/DSC, FTIR, and SEM analyzes. Results of adsorption tests, varying pH and time, suggested that the maximum amounts of drug adsorption in the NC, EC and OC were 58.29, 76.02, and 106.42 mg.g<sup>-1</sup> (pH=1.0, 28 °C), respectively. For each kinetic study of the adsorption of the drug DXZ in NC, EC, and OC, the pseudo-second-order model showed the best fit for the adsorption process due to the highest values of the correlation coefficient with a value of  $R^2=0.9999$  for both NC and EC and  $R^2=0.9998$  for OC. Taken altogether, these results suggested a rate-limiting event of chemisorption of the drug on the surface of the OC material. Therefore, the present study showed that the OC is a promising material for use in the incorporation of drug molecules with a structure similar to doxazosin.

## REFERENCES

- [1] T. Azuma, K. Otomo, M. Kunitou, M. Shimizu, K. Hosomaru, S. Mikata, M. Ishida, K. Hisamatsu, A. Yunoki, Y. Mino, T. Hayashi, *Sci. Total Environ.* **657** (2019) 476.
- [2] D. White, D.J. Lapworth, W. Civil, P. Williams, *Environ. Pollut.* **249** (2019) 257.
- [3] E.C. Back, C.J. Flanagan, L.J. Jones, I. Augur, L.A. Peterson, S. Young-McCaughan, W.D. Shirley, A. Henschel, E.J. Joseph, T.B. Litz, K.A. Hancock, D.J. Roache, J. Mintz, S.J. Wachenh, M.T. Keane, K. Brady, *Contemp. Clin. Trials* **73** (2018) 8.
- [4] R. Baccar, J. Bouzid, M. Feki, A. Montiel, J. Hazard. *Mater.* **162** (2009) 1522.
- [5] M. Mahmoud, M.G. Nabil, M.N. El-Mallah, I.H. Bassiouny, S. Kumar, M.T. Abdel-Fattah, *J. Ind. Eng. Chem.* **37** (2016) 156.
- [6] G.G. Stavropoulos, A.A. Zabaniotou, *Microporous Mesoporous Mater.* **83** (2005) 79.
- [7] F. Wang, X. Ren, H. Sun, L. Ma, H. Zhu, J. Xu, *Bioresour. Technol.* **219** (2016) 458.
- [8] C. Tournassat, I.C. Bourg, C.I. Steefel, F. Bergaya (Eds.), "Natural and engineered clay barriers", *Developments in clay science* **6** Elsevier, Amsterdam (2015).
- [9] M. Balat, *Energy Convers. Manag.* **52** (2011) 858.
- [10] M.D. Bila, M. Dezotti, *Quim. Nova* **26** (2003) 523.
- [11] S.C.C. Maura, S.F.S. Maria, B.S.D. Roosevelt, J.A.A. Edgar, O.A. Josy, S.C.M.R. Maria, F.G. Maria, F.S.C. Edson, *Int. J. Biol. Macromol.* **161** (2020) 927.
- [12] X.M.C. Katiane, S.F.S. Maria, O.A. Josy, L.B. Adão, F.G. Maria, F.S.C. Edson, *Appl. Clay Sci.* **119** (2016) 347.
- [13] H. Hayashi, R. Otsuka, N. Imai, *Am. Mineral.* **54** (1969) 1624.
- [14] A. Bourliva, K.A. Sikalidis, L. Papadopoulou, M. Betsiou, K. Michailidis, C. Sikalidis, A. Filippidis, *Clay Miner.* **53** (2018) 1.
- [15] L.B. de Paiva, A.R. Morales, F.R.V. Díaz, *Cerâmica* **54**, 330 (2008) 213.

- [16] L.B. de Paiva, A.R. Morales, F.R.V. Díaz, *Appl. Clay Sci.* **42** (2008) 24.
- [17] G.L. Dotto, M.L.G. Vieira, J.O. Gonçalves, L.A. Pinto, *Quim. Nova* **34** (2011) 1199.
- [18] F.W. Alvarenga, P.B. Martelli, H.F. Gorgulho, “Carvões ativados utilizando palha de milho como matéria prima, obtenção e uso”, PI0804435-0 A2, INPI (2010).
- [19] C.A.I. Aguilar, J.B.I. Lladó, M.C.O. Miguel, “Method for obtaining polymorph a from doxazosine mesylate”, US Patent 6525195 B1 (2003).
- [20] R.D. Joaquín, G. Teresa, P. Patricia, C.C.M. Eduardo, *Desalination* **269** (2011) 238.
- [21] D. Turollo, M. Oliveira, G. Lima, *Rev. Geonorte* **10** (2014) 36.
- [22] E.V.D. Gomes, L.L.Y. Visconde, E.B.A.V. Pacheco, *Cerâmica* **56**, 337 (2010) 44.
- [23] Y. Shengjun, L. Guozheng, G. Aijuan, M. Huihui, *Appl. Clay Sci.* **285** (2013) 726.
- [24] Y.S. Ho, G. Mckay, *Biochemistry* **34** (1999) 465.
- [25] Y.S. Ho, G. Mckay, *Water Res.* **34** (2000) 742.
- [26] P.S. Santos, *Tecnologia de argilas* **1**, Edgard Blücher, S. Paulo (1975) 70.
- [27] C.P.F. dos Santos, D.M.A. Melo, M.A.F. Melo, E.V. Sobrinho, *Cerâmica* **48**, 308 (2002) 178.
- [28] E. Nishikawa, A.F. De Almeida Neto, M.G.A. Vieira, *Adsorpt. Sci. Technol.* **30** (2012) 772.
- [29] R.A. Rojas-Ramires, M.H. Maciel, R.C.O. Romano, I.R.G. Pileggi, A.C. Vieira-Coelho, *Appl. Clay Sci.* **170** (2019) 105.
- [30] O. Duman, S. Tunç, T.G. Polat, *Appl. Clay Sci.* **109** (2015) 32.
- [31] L. Chen, P. Wu, M. Chen, X. Lai, Z. Ahmed, N. Zhu, Z. Dang, Y. Bi, T. Liu, *Appl. Clay Sci.* **159** (2018) 82.
- [32] M.V.S. Fernandes, L.R.D. da Silva, *Cerâmica* **60**, 354 (2014) 205.
- [33] F. Mazloomi, M. Jalali, *Environ. Monit. Assess.* **189** (2017) 415.
- [34] D.S. Moraes, E.M.S. Rodrigues, C.N. Lamarão, G.T. Marques, A.F.S. Rente, *J. Hazard. Mater.* **366** (2019) 38.
- [35] M.A. Franco, A.A. Liso, V.G. Serrano, *Fuel Process. Technol.* **92** (2011) 205.
- [36] F. Mazloomi, M. Jalali, *Catena* **176** (2019) 180.
- [37] A.P.O. Da Silva, J.V. De Melo, S.B.C. Pergher, *Perspectiva* **41**, 155 (2017) 100.
- [38] Z. Fu, T. Liu, X. Kong, Y. Liu, J. Xu, B. Zhang, H. Chen, Z. Chen, *Mater. Lett.* **238** (2019) 178.
- [39] M.A. Franco, A.A. Liso, V.G. Serrano, *Fuel Process. Technol.* **92** (2011) 205.
- [40] M. Yu, M. Gao, T. Shen, J. Wang, *Colloids Surf. A Physicochem. Eng. Asp.* **553** (2018) 611.
- [41] S.S.G. Santos, M.B.B. Pereira, R.K.S. Almeida, A.G. Souza, M.G. Fonseca, M. Jaber, *J. Hazard. Mater.* **306** (2016) 418.
- [42] X. Yu, C. Wei, L. Ke, Y. Hu, X. Xie, H. Wu, *J. Hazard. Mater.* **180** (2010) 507.
- [43] J. Tang, Z.F. Yang, Y.J. Yi, *Procedia Environ. Sci.* **13** (2012) 2187.
- [44] O. Dlugosz, M. Banach, *Appl. Sci.* **8** (2018) 7.
- [45] G.Z. Kyzas, N.K. Lazaridis, A.Ch. Mitropoulos, *Chem. Eng. J.* **190** (2012) 148.
- [46] W. Yang, T. Peng, Z. Miao, *Adv. Mater. Res.* **96** (2010) 6.
- [47] A. Fakhri, S. Adami, *J. Taiwan Inst. Chem. Eng.* **45**, 3 (2014) 1006.
- [48] P. Ding, K.L. Huang, G.Y. Li, Y.F. Liu, W.W. Zeng, *Int. J. Biol. Macromol.* **39** (2006) 227.
- (*Rec. 05/05/2021, Rev. 20/08/2021, Ac. 15/09/2021*)